Analytical Modeling and Numerical Simulation of $Hg_{1-x}Cd_xTe$ Based $N^+n^0p^+$ Photodetector for MWIR Free Space Optical Communication

A.D.D. Dwivedi[1,*] and P. Chakrabarti[2]

[1]*IMS Lab, University of Bordeaux 1, France*

[2]*Motilal Nehru National Institute of Technology, Allahabad-211004, India*

Abstract: This paper reports an analytical modeling and numerical simulation of N^+-$Hg_{0.59}$ $Cd_{0.41}Te$ /n^0 $Hg_{0.65}$ $Cd_{0.35}Te$ /p^+-$Hg_{0.65}$ $Cd_{0.35}$ $N^+n^0p^+$ photodetector for operation in medium wavelength infrared region (MWIR) for free space optical communication. The photodetector has been studied in respect of quantum efficiency, responsivity and detectivity by analytical method using closed form equations. Also numerical simulation has been performed using device simulation software ATLAS™ for obtaining the energy band diagram, electric field profile, doping profile, quantum efficiency, responsivity and detectivity**.** The photodetector exhibits a high value of quantum efficiency~93%, responsivity~2.86A/W and detectivity~1.33×10^{11} $mHz^{1/2}W^{-1}$ at wavelength of operation 3.8 µm.

Keywords: Medium wave length infrared region (MWIR), Photodetector, Numerical simulation, Spectral response, Quantum efficiency, Responsivity and Detectivity.

INTRODUCTION

The key component of an optical receiver is the photodetector which converts incoming optical signal to the corresponding electrical signal. For successful implementation of high speed optical communication systems it is necessary to develop suitable photodetectors. An extensive research work has been carried out world-wide over the past decades for exploring various semiconductor photodetectors. There are two basic mode of optical communication *e.g*. guided optical communication that uses optical fibers as the channel and the unguided optical communication that uses free space as the channel. The latter is also known as free space optical communication. In guided optical communication system, the fibers used for optical communication are primarily made of glass (silica) which offers low loss in the near infrared (NIR) region, typically 0.85µm to 1.65 µm. As the loss of glass increases significantly in the longer wavelength region optical fiber communication has not been developed so for, for operation in this region. Free space optical communication on the other hand has several atmospheric windows in the near infrared region as well as in the medium wavelength infrared region (MWIR) and long wavelength infrared region (LWIR). For terrestrial applications, certain strategic atmospheric attenuation windows *e.g*., 3.8 µm in MWIR and 10.6µm in LWIR have been chosen for development of free space optical links. $Hg_{1-x}Cd_xTe$ can be used to develop detectors for operation at these wavelength regions. The mole fraction of cadmium in HgCdTe can be adjusted suitably to tailor the energy bandgap of the material so as to match with the wavelengths corresponding to the MWIR and LWIR atmospheric windows [1]. Analytical modeling and ATLAS TCAD tool based numerical simulation of $Hg_{1-x}Cd_xTe$ based photodetectors for operation in LWIR region have been reported in [2-6], InGaAs based photodetector for operation in NIR region is reported in [7], sensitivity analysis of the front end receivers based on $Hg_{1-x}Cd_xTe$ based photodetectors has been reported in [8-10] and some photovoltaic behavior of Polycarbazole based polymers have been reported in [11-12] for UV-visible region. Numerical simulation approach has also been applied to Pentacene based organic TFTs [13]. In view of above, numerical simulation using ATLAS TCAD from Silvaco international can be utilized for numerical simulation of $Hg_{1-x}Cd_xTe$ based MWIR photodetector. In this paper we report analytical and ATLAS™ simulation results of the proposed N^+-$Hg_{0.59}$ $Cd_{0.41}Te$ /n^0 $Hg_{0.65}$ $Cd_{0.35}Te$ /p^+-$Hg_{0.65}$ $Cd_{0.35}Te$ $N^+n^0p^+$ photodetector for free space optical communication at 3.8µm MWIR atmospheric window.

TCAD SIMULATION METHODOLOGY

The proposed $N^+n^0p^+$ (p-i-n) device structure is shown in Figure **1**. Various parameters used in the computations were taken from reference [14-23]. It consists of highly doped p^+-$Hg_{0.65}$ $Cd_{0.35}Te$ over lightly doped n^0 $Hg_{0.65}$ $Cd_{0.35}Te$ which is virtually grown on highly doped N^+-$Hg_{0.59}$ $Cd_{0.41}Te$ on a suitable substrate such as CdZnTe or sapphire. The N^+-$Hg_{0.59}$ $Cd_{0.41}Te$ acts as window and incident light is absorbed in n^0

*Address correspondence to this author at the IMS Lab, University of Bordeaux 1, France; Tel: +33 7534 22024;
E-mail: adddwivedi@gmail.com

E-ISSN: 2408-977X/15

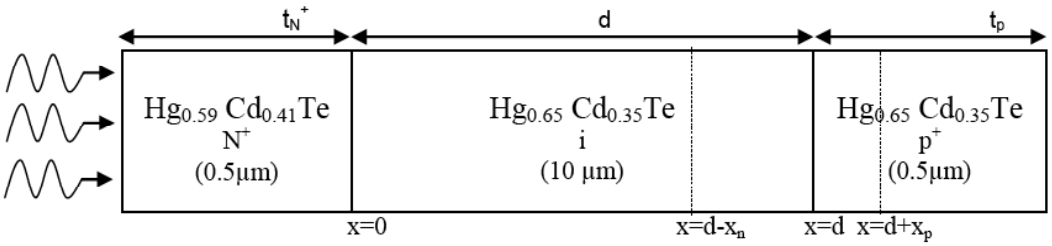

Figure 1: Schematic structure of the proposed N^+-$Hg_{0.59}$ $Cd_{0.41}Te$ /n^0 $Hg_{0.65}$ $Cd_{0.35}Te$ /p^+-$Hg_{0.65}$ $Cd_{0.35}Te$ photodetector.

$Hg_{0.65}$ $Cd_{0.35}Te$ and p^+-$Hg_{0.65}$ $Cd_{0.35}Te$ regions. The electrical and optical behavior of the HgCdTe based $N^+n^0p^+$ photodetector has been studied using a finite element based method (FEM) utilizing a commercial numerical device simulator ATLAS™. The numerical simulation of $N^+n^0p^+$ photodetector has been carried out for non degenerate semiconductor and parabolic shape of conduction band. The simulation involves solution of five coupled equations using Newton's iteration technique. The set of fundamental equations comprise of Poisson's equation, the continuity equations and the transport equations. The solution of Poisson's equation and continuity equation that are a set of coupled, partial differential equations which is solved numerically with the help of ATLAS software for obtaining terminal characteristics of the conventional devices is as below

Poisson's Equation

Poisson's Equation relates variations in the electrostatic potential to local charge densities. It is mathematically described by the following relation [5, 13]

$$\nabla.(\varepsilon\nabla\psi) = -\rho \tag{1a}$$

$$\nabla.(\varepsilon\nabla\psi) = -q\left(p - n + N_d^+ - N_a^-\right) \tag{1b}$$

where ϕ is the electrostatic potential, ρ is the local space charge density, ε is the local permittivity of the semiconductor (F/cm), p is the hole density (cm^{-3}), n is the electron density (cm^{-3}), N_d^+ is the ionized donor density (cm-3) and N_a^- is the ionized acceptor density (cm^{-3}).

Continuity Equations

For electrons and holes, the continuity equations are defined as follows [5, 13]

$$\frac{\partial n}{\partial t} = \frac{1}{q}\nabla.J_n + G_n - R_n \tag{2}$$

$$\frac{\partial p}{\partial t} = -\frac{1}{q}\nabla.J_p + G_p - R_p \tag{3}$$

where n and p are the electron and hole concentrations, J_n and J_p are the electron and hole current densities, G_n (R_n) and G_p (R_p) are the generation (recombination) rates for the electrons and holes, respectively and q is the fundamental electronic charge.

Transport Equations

The Current density equations are obtained by using the "drift-diffusion" charge transport model. The drift-diffusion model is described as follows

$$J_n = qn\mu_n \mathrm{E}_n + qD_n\nabla n \tag{4}$$

$$J_p = qn\mu_p \mathrm{E}_p - qD_p\nabla \mathrm{p} \tag{5}$$

where μ_n and μ_p are the electron and hole mobilities, D_n and D_p are the electron and hole diffusion constants, E_n and E_p are the local electric fields for electrons and holes, respectively, and ∇ n and ∇ p are the three dimensional spatial gradient of n and p.

Analytical Modeling of Quantum Efficiency

For computation of quantum efficiency (η) of N^+-$Hg_{0.59}$ $Cd_{0.41}Te$ /n^0 $Hg_{0.65}$ $Cd_{0.35}Te$ /p^+-$Hg_{0.65}$ $Cd_{0.35}Te$ $N^+n^0p^+$ photodetector we have taken into account three major components. These components arise from the contribution of the three regions *e.g.*, neutral p-region *(η_p),* neutral n^0-region *(η_n)*, and the depletion region *(η_{dep})*. The optical generation rate of electron-hole pairs, as a function of distance x from the surface can be written as

$$G_n(x) = \frac{\alpha_n(\lambda)\left(1-R_{N^+}\right)\left(1-R_{n^0}\right)P_{opt}}{Ah\nu}\exp\left(-\alpha_n(\lambda)x\right) \tag{6}$$

$$G_p(x) = \frac{\alpha_p(\lambda)\left(1-R_{N^+}\right)\left(1-R_{n^0}\right)\left(1-R_{p^+}\right)P_{opt}}{Ah\nu}\exp\left(-\alpha_p(\lambda)x\right) \tag{7}$$

where $\alpha(\lambda)$ is the optical absorption coefficient of the

material which is a function of wavelength λ, R_{N^+}, R_{n^0} and R_{p^+} are the Fresnel reflection coefficient at N^+, n^0 and p^+ interfaces, P_{opt} is the incident optical power, v is the frequency of radiation and A is the device area. By solving continuity equations using appropriate boundary conditions at N^+-$Hg_{0.59}$ $Cd_{0.41}Te$ /n^0 $Hg_{0.65}$ $Cd_{0.35}Te$ hetero interface and at p^+ region and metal contact for holes and electrons respectively the quantum efficiency components can be obtained as discussed in[4]. The net quantum efficiency can be written as

$$\eta = \eta_n + \eta_p + \eta_{dep} \tag{8}$$

Modeling of Specific Detectivity

The most important figure of merit of the photodetector for use in optical communication is the specific detectivity D^*, which depends on the wavelength of incident light λ, the quantum efficiency η and zero bias resistance area product, R_0A. As the dark current of the detector is contributed by three major components *e.g*., diffusion, generation-recombination and tunneling (which includes trap assisted tunneling (TAT) and band to band tunneling (BTB)), the detectivity of the photodetector under consideration has been estimated from the net value of R_0A product arising out of these mechanism. The dark current of the $N^+n^0p^+$ photodetector has been modeled here by considering (i) the diffusion of thermally generated carriers from neutral regions, I_{DIFF} (ii) generation-recombination of carriers in the depletion region, I_{GR} and (iii) tunneling of carriers through barriers, I_{TUN}. In order to generalize the analysis, we have however considered both trap assisted tunneling (TAT) as well as band-to-band tunneling (BTB). The tunneling component of current thus constitutes two components *e.g*. I_{TAT} arising from the trap assisted tunneling and I_{BTB} arising out of band-to-band tunneling. The dark current and resistance area product modeling has been performed using modeling equation as in [4]. The net current can be written as

$$I=I_{DIF}+I_{GR}+I_{TAT}+I_{BTB} \tag{9}$$

The net value of the resistance area product can be written as

$$\frac{1}{(RA)_{NET}} = \frac{1}{(RA)_{DIFF}} + \frac{1}{(RA)_{GR}} + \frac{1}{(RA)_{TAT}} + \frac{1}{(RA)_{BTB}} \tag{10}$$

The specific detectivity of the photodetector which is a function of the applied voltage can be written as

$$D^* = \frac{q\eta\lambda}{hc}\sqrt{\frac{(R_0A)_{NET}}{4kT}} \tag{11}$$

Responsivity

The current responsivity (R) of the photodetector is given as

$$R = \frac{\eta q\lambda}{hc} \tag{12}$$

RESULTS AND DISCUSSIONS

Numerical computations have been carried out for theoretical characterization of N^+-$Hg_{0.59}$ $Cd_{0.41}Te$ /n^0 $Hg_{0.65}$ $Cd_{0.35}Te$ /p^+-$Hg_{0.65}$ $Cd_{0.35}Te$ $N^+n^0p^+$ photodetector for operation at temperature 78 K. The mole fraction of cadmium in the ternary MCT material has been calculated so that the bandgap energy of the material corresponds to the long wavelength cut-off value of 3.8 μm for MWIR free space optical communication. The band gap of $Hg_{1-x}Cd_xTe$ as a function of temperature, T and alloy composition, x is included in the simulation model using the following empirical formula [14]

$$E_g = -0.302 + 1.93x - 0.810x^2 + 0.832x^3 + 5.35\times10^{-4}(1-2x)\left(\frac{-1822+T^3}{255.2+T^2}\right) \tag{13}$$

The intrinsic carrier concentration was calculated using the following expression [15]

$$n_i = \left(\begin{array}{l} 5.24256 - 3.57290\,x - 4.74019\times10^{-4}T + \\ 1.25942\times10^{-2}xT - 5.77046\,x^2 - 4.24123\times10^{-6}T^2 \end{array}\right)$$

$$\times10^{14}E_g^{\,3/4}T^{3/2}\exp\left(\frac{-E_g}{2kT}\right) \tag{14}$$

where k is Boltzmann 's constant. From Kane band model the hole effective mass is taken as m_h^*=0.55 m_0 and electron effective mass has been computed following [16] as

$$\frac{m_0}{m_n^*} = 1 + 2F + \frac{E_p}{3}\left(\frac{2}{E_g} + \frac{1}{E_g+\Delta}\right) \tag{15}$$

where E_p =19 eV, F=-0.8 and Δ =1.0 eV. The electron mobility has been computed using the empirical formula given by [14]

$$\mu_n = \frac{9\times10^4\,s}{T^{2r}}\ \text{m}^2/\text{vs} \tag{16}$$

where $r=(0.2x)^{0.6}$ and $s=(0.2/x)^{7.5}$ which are valid in

composition range $0.2 \leq x \leq 0.6$ and temperature range T >50K.

The hole mobility has been assumed to be of the form [14]

$$\mu_n = \mu_0 \left[1+\left(\frac{p}{1.8\times10^{23}}\right)^2\right]^{-1/4} \quad (17)$$

where μ_0 = 0.044 m^2/Vs

The absorption coefficient of $Hg_{1-x}Cd_xTe$ for optical carrier generation can be calculated within the Kane model, including the Moss-Burstein shift .For photon energy E< E_g (tail region), $\alpha < \alpha_g$, the absorption coefficient obeys the rule [17-18]

$$\alpha = \alpha_0 \exp\left(\frac{\delta(E-E_0)}{kT}\right) \quad (18)$$

And for photon energy E> E_g (Kane region), the absorption coefficient obeys the rule [20]

$$\alpha = \alpha_g \exp\left(\beta\left(E-E_g\right)\right)^{1/2} \quad (19)$$

where α_0 is the fitting parameter and

$$E_0 = -0.355 + 1.77x \quad (20)$$

$$\frac{\delta}{kT} = \frac{\ln\alpha_g - \ln\alpha_0}{E_g - E_0} \quad (21)$$

$$\alpha_g = -65 + 1.88T + (8694 - 10.315T)x \quad (22)$$

$$\beta = -1 + 0.083 + (21 - 0.13T)x \quad (23)$$

The expressions of the high frequency dielectric constant ε_∞ and static dielectric constant ε_s are obtained as a function of x as [14]

$$\varepsilon_\infty = 15.2 - 15.6x + 8.2x^2 \quad (24)$$

$$\varepsilon_s = 20.5 - 15.6x + 5.7x^2 \quad (25)$$

The light has been assumed to be incident from substrate side through N^+-$Hg_{0.59}$ $Cd_{0.41}Te$. The incident photons with energy higher than the bandgap of $Hg_{0.65}$ $Cd_{0.35}Te$ are absorbed in both the n^0 and p^+ regions. The doping of the regions has been taken analytically uniform for all regions in the above simulation. In calculation of mobility the concentration dependent ANALYTIC model has been considered. For the simulation of dark current, associated with $N^+n^0p^+$ photodetector, AUGER, SRH and OPTICAL (band-to-band) models have been taken into account for recombination mechanisms modeling. Band-to-band standard tunneling model has been considered for tunneling mechanism. The surface recombination process at the contacts and heterointerface has been taken into account in simulation and also in analytical model. The quality of the interface has been characterized in terms of surface recombination velocity. We have taken into account the Fermi-Dirac statistics for parabolic shape of conduction band in all the calculations of carrier and doping densities. For the simulation of dark current associated with $N^+n^0p^+$ photodetector, the optical, SRH, Augur and surface recombination rates are given as given in [2]. The variation of quantum efficiency, current responsivity and specific detectivity with wavelength at 78 K have been computed from the above mentioned model. The proposed photodetector structure has also been simulated using device simulation software ATLAS™ from SILVACO® international. A program was developed separately for calculation of various characteristics of the photodetector using MATLAB platform by choosing appropriate material parameters. The simulated results of $N^+n^0p^+$ photodetector were obtained by developing program in DECKBUILD window interfaced with ATLAS for N^+-$Hg_{0.59}$ $Cd_{0.41}Te$ /n^0 $Hg_{0.65}$ $Cd_{0.35}Te$ /p^+-$Hg_{0.65}$ $Cd_{0.35}Te$ $N^+n^0p^+$ photodetector at 78K. Instead of the graded doping the numerical model includes a uniform doping profile. Once the physical structure of photodetector is built in ATLAS, the properties of the material used in device must be defined. A minimum set of material properties data includes, bandgap, dielectric constant, electron affinity, densities of conduction and valance band states, electron and hole mobility, optical recombination coefficient, and an optical file containing the wavelength dependent refractive index, n [7, 24-25] and extinction coefficient *K* [7, 24-25] for the used materials. The wavelength dependent values of extinction coefficient K is computed from the relation [7]

$$K = \frac{\alpha\lambda}{4\pi} \quad (26)$$

The energy band diagram has been simulated from BLAZE, which is interfaced with ATLAS is a general purpose 2-D device simulator for III-V, II-VI materials, and devices with position dependent band structure (i.e., heterojunctions) [25]. BLAZE accounts for the effects of positionally dependent band structure by

modifications to the charge transport equations. Equilibrium energy band diagram for electrons is shown in Figure **2**, It has been simulated using BLAZE which shows the notch and spike at the heterointerface for estimation of amount of discontinuity in the conduction band and valence band. Doping concentration inside the device along with the device structure is shown in Figure **3**. Equilibrium condition electric field profile of the photodetector is shown in Figure **4**. Doping profile of the device is shown in Figure **5**, which shows, position dependent electron and hole concentration inside the device in different regions. The optical characteristics of the device have been studied by using LUMINOUS tool of ATLAS device simulator. LUMINOUS, the optoelectronic simulation module in ATLAS, determines the photogeneration at each mesh point in an ATLAS structure by performing two simultaneous calculations. The refractive index n is used by LUMINOUS to perform an optical ray trace in the device. Difference in n values across the material boundaries determines the rate of light transmission and reflection. By following the path of light from the source to a mesh point, Luminous is able to determine the optical intensity at that point. Together, these simulations provide for wavelength dependent photogeneration throughout the photodetector [7, 24-25]. The spectral response of the photodetector showing the variation of actual value of cathode current, source photocurrent and available photocurrent with wavelength is shown in Figure **6**. Cathode current increases with wavelength of operation and attains a maximum value at λ=3.8μm and there is a sharp fall beyond λ=3.8μm which is longer cut off wavelength for the proposed composition of the $Hg_{1-x}Cd_xTe$, which is absorbing layer in the proposed photodetector. All the results discussed above have been obtained by ATLAS TCAD simulation. Variation of quantum efficiency of $N^+n^0p^+$ photodetector with wavelength of operation as obtained from analytical model and ATLAS TCAD simulation at a bias voltage of 0.5V is shown in Figure **7**. From this figure it is clear that there is a good agreement in the quantum efficiency value estimated analytically and that computed on the basis of ATLAS simulation. The device exhibits very high quantum efficiency ~ 93% which attributes the high detectivity of the photodetector. The variation of responsivity of the photodetector with wavelength of operation is shown in Figure **8**. From this figure we can see that there is a very good matching between responsivity obtained from analytical model and those obtained from ATLAS TCAD simulation. The device exhibits very high values of responsivity ~2.86A/W at wavelength 3.8μm and a bias voltage of 0.5V. Figure **9** shows variation of specific detectivity with wavelength of operation, obtained by analytical model and also by ATLAS TCAD simulation which indicate that the order of the detectivity values as obtained by the two methods are very close. The device exhibits very high value of specific detectivity~1.33×10^{11} $mHz^{1/2}W^{-1}$at wavelength of operation 3.8μm.

CONCLUSION

We proposed an N^+-$Hg_{0.59}$ $Cd_{0.41}Te$ /n^0 $Hg_{0.65}$ $Cd_{0.35}Te$ /p^+-$Hg_{0.65}$ $Cd_{0.35}Te$ $N^+n^0p^+$ photodetector for free space optical communication. The performance of the device has been examined by developing an analytical model for the quantum efficiency, responsivity and detectivity and results obtained from analytical model have been compared and contrasted by those obtained from ATLAS™ device simulation software from SILVACO® international. There is a very

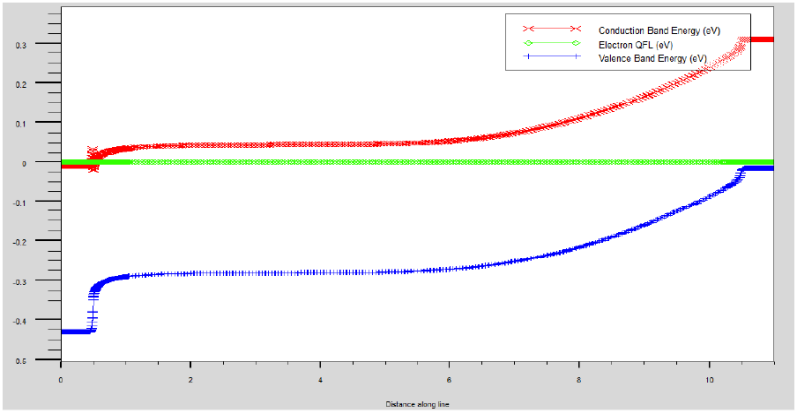

Figure 2: Equilibrium energy band diagram.

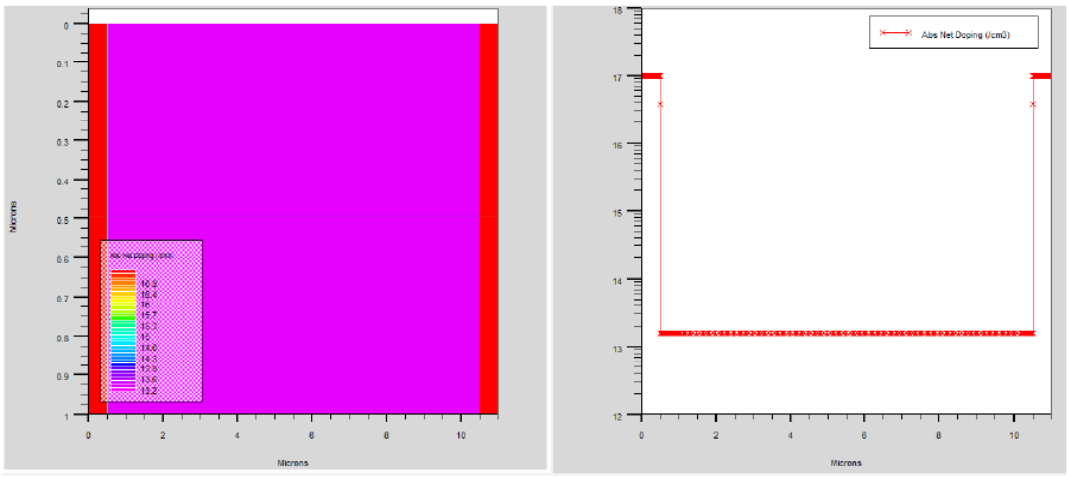

Figure 3: Doping concentration along the structure.

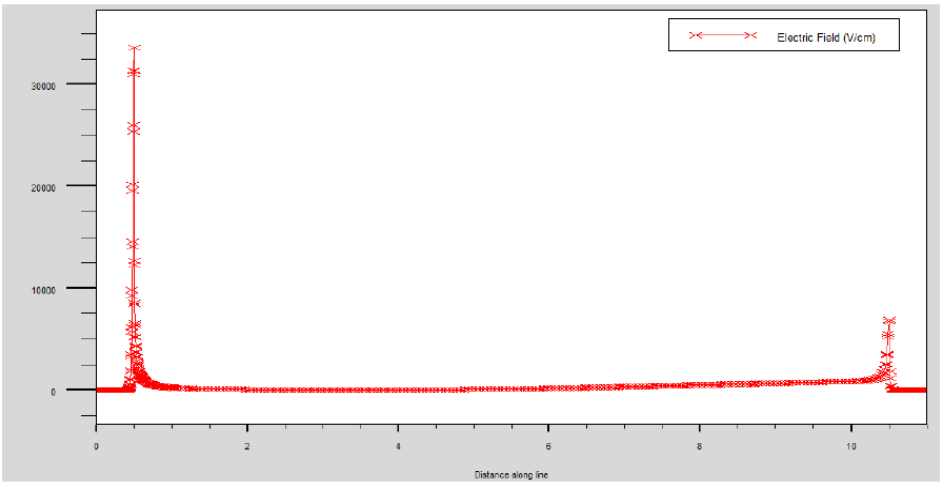

Figure 4: Zero bias electric field profile of $N^+n^0p^+$ photodiode.

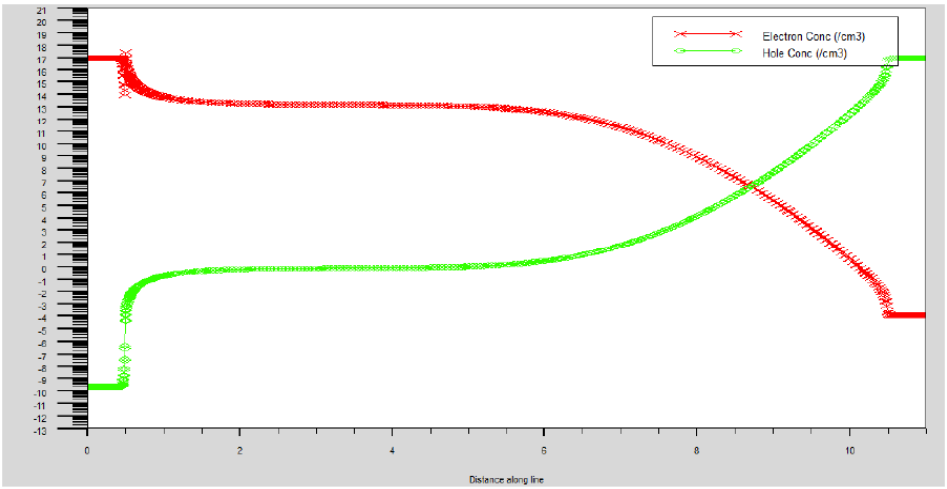

Figure 5: Electron and hole concentration profile.

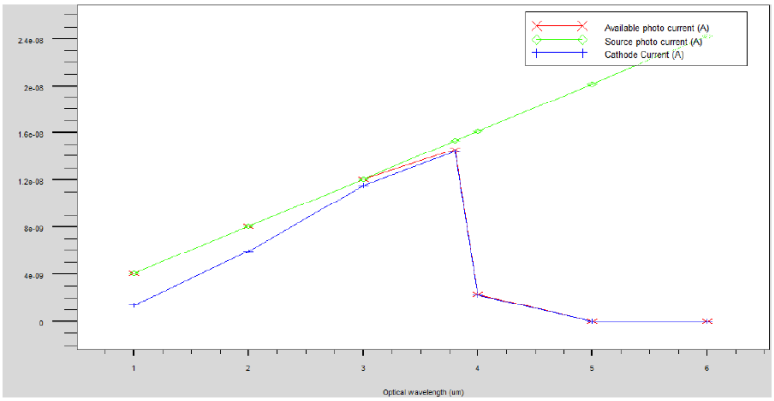

Figure 6: Spectral response of $N^+n^0p^+$ photodiode.

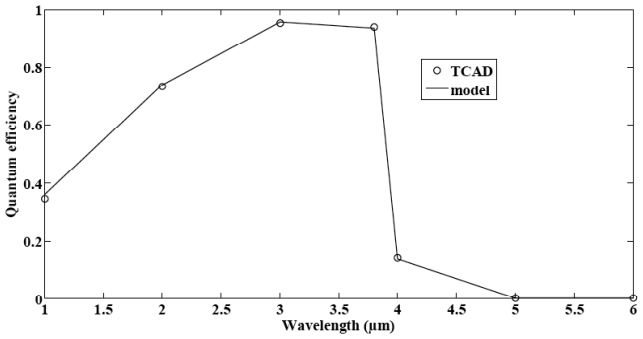

Figure 7: Variation of Quantum Efficiency of $N^+n^0p^+$ photodetector with wavelength.

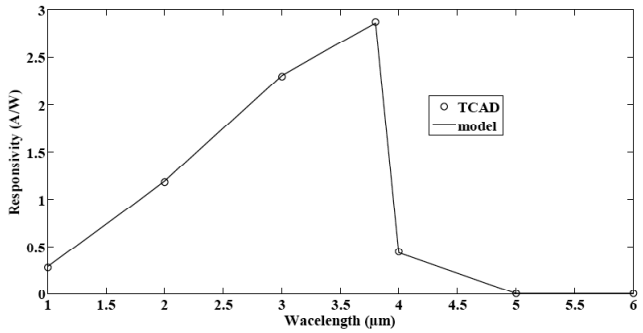

Figure 8: Variation of Responsivity with wavelength.

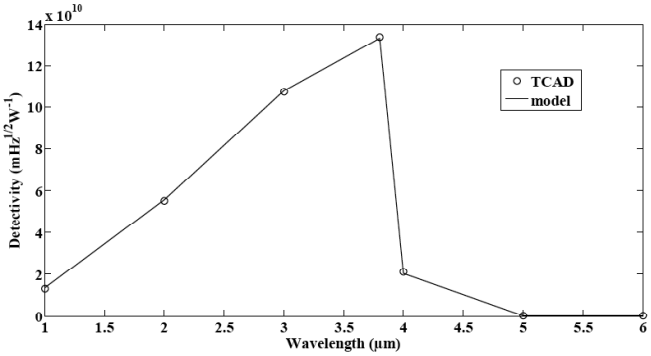

Figure 9: Variation of Detectivity of $N^+n^0p^+$ photodiode with wavelength.

good agreement between results obtained by analytical model and those obtained from ATLAS simulation. The device exhibited very high quantum efficiency~93%, responsivity~2.86A/W and detectivity~1.33×10^{11} $mHz^{1/2}W^{-1}$ at wavelength of operation 3.8 μm. While the analytical model explores various physical mechanisms that shape the device characteristics, the simulation make use of advanced numerical technique to extract the performance of the $N^+n^0p^+$ structure.

REFERENCES

[1] Dwivedi ADD, Chakrabarti P. "Modeling and analysis of photoconductive detectors based on Hg1- x Cd x Te for free space optical communication," Optical and Quantum Electronics 2007; 39: 627-641. http://dx.doi.org/10.1007/s11082-007-9122-4

[2] Dwivedi ADD. "Analytical Modeling and Numerical Simulation of P+-Hg0.69 Cd0.31Te/n-Hg0.78Cd0.22Te/CdZnTe Heterojunction Photodetector for LWIR Free Space Optical Communication System," Journal of Applied Physics 2011; 110: 043101. http://dx.doi.org/10.1063/1.3615967

[3] ADD. Dwivedi, "Analytical Modeling and ATLAS Simulation of p+-Hg0.78 Cd0.22Te/n-Hg0.78Cd0.22Te/CdZnTe Homojunction Photodetector for LWIR Free Space Optical Communication System," Journal of Electron Devices 2011; 9: 396-404.

[4] Dwivedi ADD, Chakrabarti P. "Analytical Modeling and ATLAS Simulation of N+-Hg0.69 Cd0.31Te /n0- Hg0.78 Cd0.22Te/p+Hg0.78 Cd0.22Te p-i-n Photodetector for Long wavelength Free Space Optical Communication," Optoelectronics and Advanced Materials-Rapid Communications (OAM-RC) 2010; 4: 480-497.

[5] Dwivedi ADD, Pranav A, Gaurav Gupta, Chakrabarti P. "Numerical Simulation of HgCdTe based simultaneous MWIR/LWIR photodetector for free space optical communication" International Journal of Advanced Applied Physics Research 2015; 2: 37-45. http://dx.doi.org/10.15379/2408-977X.2015.02.01.5

[6] Ritu Singh, Surabhi Panda, Dwivedi ADD, Chakrabarti P. "Modeling and Simulation of Photoconductive Detectors based on Hg1-xCdxTe for Free Space Optical Communication." Proc. of IRMMW-THz 2006, held at Shanghai Institute of Technical Physics, Shanghai, China, September 2006; 18-22.

[7] Dwivedi ADD, Mittal A, Agrawal A, Chakrabarti P. "Analytical Modeling and ATLAS Simulation of N+-InP/n0-In0.53Ga0.47As/p+In0.53Ga0.47As p-i-n Photodetector for Optical Fiber Communication," Infrared Physics & Technology, 2010; 53: 4: 236-245. http://dx.doi.org/10.1016/j.infrared.2010.03.003

[8] Dwivedi ADD, Chakrabarti P. "Sensitivity analysis of an HgCdTe based photovoltaic receiver for long- wavelength free space optical communication systems" Optoelectronics Letters 2009; 5: 21-25. http://dx.doi.org/10.1007/s11801-009-8123-x

[9] Dwivedi ADD, Chakrabarti P. "Sensitivity analysis of an HgCdTe based photoconductive receiver for long-wavelength free space optical communication systems," Proc. of IRMMW-THz 2007, held at Cardiff, UK, September 2-7, 2007. http://dx.doi.org/10.1109/icimw.2007.4516749

[10] Dwivedi ADD, Chakrabarti P. "Sensitivity Analysis of an Hg1-xCdxTe based Photoconductive Receiver for Long Wavelength Free space optical communication at 9.6 μm," Journal of Electron Devices 2011; 9: 390-395.

[11] Dwivedi ADD, Arun Kumar Singh, Rajiv Prakash, Chakrabarti P. "A Proposed Organic Schottky Barrier Photodetector for application in the Visible Region," Current Applied Physics, 2010; 10: 900-903. http://dx.doi.org/10.1016/j.cap.2009.10.019

[12] Arun Kumar Singh, Dwivedi ADD, Chakrabarti P, Rajiv Prakash. "Electronic and Optical Properties of Electrochemically Polymerized Polycarbazole/Aluminum Schottky Diodes," Journal of Applied Physics, 2009; 105: 114506. http://dx.doi.org/10.1063/1.3139277

[13] Dwivedi ADD. " Numerical Simulation and Spice Modeling of Organic Thin Film Transistors (OTFTs)" International Journal of Advanced Applied Physics Research, 2014; 1(2): 1421. http://dx.doi.org/10.15379/2408-977X.2014.01.02.3

[14] Rogalski A, Adamiec K, Rutokowski J. "Narrow-gap semiconductor photodiodes," SPIE Press, Bellingham, Washington, USA, 2000.

[15] Capper P, Properties of Narrow Gap Cadmium-Based Compounds, EMIS data reviews series, No. 10, INSPEC, The institution of Electrical Engineers, London, 1995.

[16] Weiler MH. "Magnetooptical properties of Hg1-xCdxTe Alloyes," in Semiconductors and Semimetals, edited by RK. Willordson And AC. Beer, Academic Press, New York 1981; 16: 119-191.

[17] Chu J, Mi Z, Tang D. "Band-to band absorption in narrow-gap Hg1-xCdxTe semiconductors," J Appl Phys Vol. 71, pp.3955-3961 (1992). http://dx.doi.org/10.1063/1.350867

[18] Chu J, li B, Liu K, Tang D. "Empirical rule of intrinsic absorption spectroscopy in Hg1-xCdxTe," J Appl Phys 1994; 75: 1234-1235. http://dx.doi.org/10.1063/1.356464

[19] Bardeen J, Blatt FJ, Hall LH. " Indirect transitions from the valence to the conduction bands,"in Photoconductivity Conference, Atlantic city 1954, pp.146-154, edited by Breackenridge R, Russel B, Hahn E. Wiley, New York (1956).

[20] Shockley W, Read WT. "Statistics of recombination of holes and electrons," Phys Rev 1952; 87: 835-842. http://dx.doi.org/10.1103/PhysRev.87.835

[21] Chakrabarti P, Gawarikar A, Mehta V, Garg D. "Effect of Trap-assisted Tunneling (TAT) on the Performance of Homojunction Mid-Infrared Photodetectors based on InAsSb," Journal of Microwaves and Optoelectronics 2006; 5(1): 1-14.

[22] Gopal V, Singh SK, Mehra RM. "Analysis of dark current contributions in mercury cadmium telluride junction diodes," Infrared Physics and Technology 2002; 43: 317-326. http://dx.doi.org/10.1016/S1350-4495(02)00159-7

[23] Chakrabarti P, Krier A, Morgan AF. "Analysis and Simulation of a Mid-Infrared P+-InAs0.55Sb0.15P0.30/n0-InAs0.55Sb0.11/N+-InAs0.55Sb0.15P0.30 Double Heterojunction Photodetector Grown by LPE," IEEE Trans. On Electron Devices 2003; 50: 2049-2058. http://dx.doi.org/10.1109/TED.2003.815604

[24] ATLAS User's manual Version 5.10.0.R, SILVACO International, Santa Clara, CA 95054, 2012.

[25] Dwivedi ADD, Chakrabarti P. "Modeling and ATLAS simulation of HgCdTe based MWIR photodetector for free space optical communication," International Conference on Recent Advances in Microwave Theory and Applications (MICROWAVE-2008), 2008; 412-415, 21-24. http://dx.doi.org/10.1109/AMTA.2008.4763197

Received on 12-10-2015 Accepted on 25-11-2015 Published on 01-12-2015

http://dx.doi.org/10.15379/2408-977X.2015.02.02.4